JACS Au
AN OPEN ACCESS JOURNAL OF THE AMERICAN CHEMICAL SOCIETY

pubs.acs.org/jacsau
Article

Engineering Oxygen-Independent NADH Oxidase Integrated with Electrocatalytic FAD Cofactor Regeneration

Mengjie Hou, Jing Yuan,* Xinyu Dong, Yingjie Wang, Shihe Yang,* and Jiali Gao*

Cite This: JACS Au 2024, 4, 3581−3592
Read Online

ACCESS | Metrics & More | Article Recommendations | Supporting Information

ABSTRACT: An electrochemically mediated enzyme process for nicotinamide adenine dinucleotide (NADH) oxidation and biosensing has been developed in which the oxygen-dependent activities of wild-type NADH oxidase are replaced by electrochemical regeneration of the flavin adenine dinucleotide (FAD) cofactor in the active site. Consequently, the present bioelectrocatalysis does not rely on a continuous oxygen supply through bubbling air or pure oxygen in biosynthetic applications, which reduces enzyme stability. The coupled electrochemical and enzymatic catalysis is achieved through a combination of enzyme immobilization on the electrode and electrochemical oxidation of $FADH_2$ in the active site mediated by the electron transfer mediator ferrocene carboxylic acid (FcCA). Furthermore, to minimize the effect of dissolved oxygen when the electrocatalytic process is exposed to air, we successfully designed mutations at the Leu40 and Cys42 sites of *Leuconostoc mesenteroides* (*Lm*NOx) to block the oxygen passage into the active site and to eliminate the native FAD cofactor regeneration half-reaction. The engineered enzymes, whose activities are significantly reduced or inactive in solution, are electrocatalytically active toward conversion of NADH to NAD^+, demonstrating successful FAD cofactor regeneration in the active site via electrochemistry. Finally, we developed two highly responsive electrochemical biosensors for NADH detection which has a superior substrate specific to standard detectors using metal electrodes, and comparable detection range and detection limit (1−3 μM).

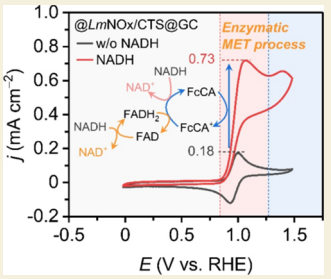

KEYWORDS: *NAD^+ regeneration, electrochemical biosensors, water-forming NADH oxidase (NOx), mediated electron transfer (MET), protein design*

INTRODUCTION

Nicotinamide adenine dinucleotide (NADH/NAD^+) and nicotinamide adenine dinucleotide phosphate (NADPH/$NADP^+$) are cofactors in a broad range of enzymatic redox reactions including those in cellular energy metabolism and biosynthesis.[1,2] Altered cellular NADH/NAD^+ ratios have been implicated in health conditions, including neurodegenerative diseases, diabetes, and cancer.[3−5] For example, elevated levels of NADH have been found in cancer cells, making it a potential biomarker for detection.[6,7] In biosynthesis, enzymatic oxidation employing the $NAD(P)^+$ cofactor provides an efficient and green route to species such as biofuels and pharmaceuticals with high levels of regio- and stereoselectivities under ambient conditions.[8−14] For example, polyol dehydrogenases, employing NAD^+ cofactor, in the polyol metabolic pathway can efficiently convert common saccharides into rare-sugar sweeteners with similar taste but only a fraction of the calorific value of sucrose.[15,16] Coupled with the dehydrogenase processes, a NAD(P)H oxidase (NOx) can be used to regenerate the oxidative form of the cofactor, in which oxygen is the oxidant with water as the byproduct. Although such an enzyme-couple would seem to be ideal, gas−liquid interface due to bubbling air or pure oxygen can affect enzyme stability, imposing critical restrictions in practice.[17−20] Unlike enzymatic and electrocatalytic regeneration of the reduced form of NADH, which have been thoroughly investigated and well established, e.g., the use of formate dehydrogenase and glucose dehydrogenase, the process to regenerate NAD^+ is still far from being solved.[21−25] It is of interest to develop an alternative, oxygen-free process to regenerate the oxidized cofactor $NAD(P)^+$ in biosynthesis. Such processes can also be engineered as a high-performance NADH detection method. In this study, we report a computation-aided design and experimental investigation of an electrochemically mediated enzyme process that converts NADH to NAD^+ by altering the native reaction pathways of NADH oxidase from *Leuconostoc mesenteroides* (*Lm*NOx) without mixing gaseous oxygen.

NADH oxidases (NOx),[26,27] lipoamide dehydrogenases,[15] and diaphorase enzyme complexes[15,28,29] are enzymes possessing NADH oxidation activities. In recent years, a particular subclass of water-forming NOx has attracted attention in biosynthetic applications.[30−33] The flavoprotein

Received: June 21, 2024
Revised: July 31, 2024
Accepted: August 1, 2024
Published: August 21, 2024

Scheme 1. Enzymatic (A) and Bioelectrocatalytic (B) Oxidation of Nicotinamide Adenine Dinucleotide (NADH)[a]

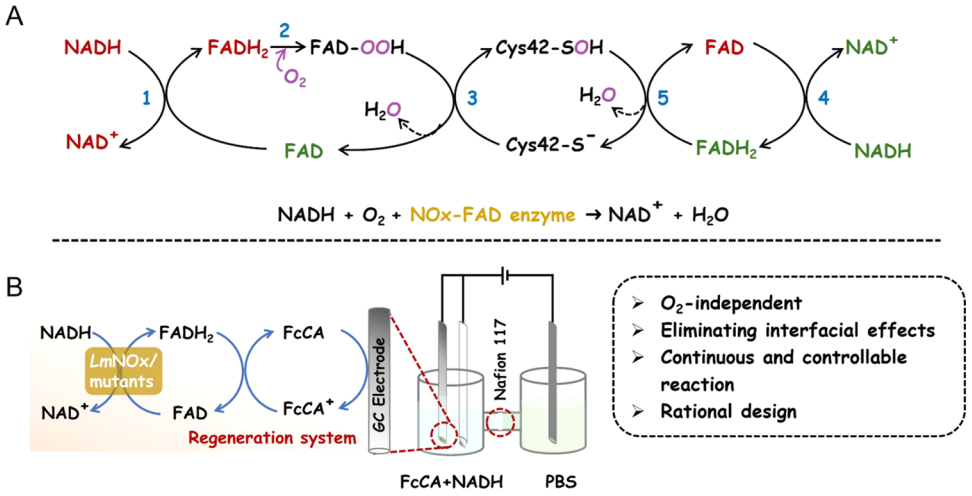

[a]In (A), the enzymatic cycle of the wild-type NADH oxidase (NOx) consists of two reaction sequences, each of which regenerates the oxidized form of FAD to catalyze the conversion of one molecule of NADH to NAD^+. Direct oxidation of the reduced form of $FADH_2$ by molecular oxygen produces the reactive FAD (green) and the Cys42-SOH intermediate, corresponding to steps **1**, **2**, and **3**. The "green" FAD cofactor is then reduced to $FADH_2$ by oxidizing a second NADH to NAD^+ (green), which is regenerated (FAD in maroon) by Cys42-SOH in reaction steps **4** and **5**. The "maroon" FAD is used in step **1** (green) to complete the catalytic cycle, producing a net of two molecules of NAD^+. In the bioelectrocatalytic process in (B), regeneration of the reactive FAD cofactor is replaced by ferrocene carboxylic acid (FcCA) mediated electrooxidation, using either wild-type NOx or an engineered enzyme without oxygen dependence.

L. mesenteroides NOx is a dimeric enzyme that utilizes flavin adenine dinucleotide (FAD) as a cofactor in NADH oxidation.[34] Each subunit of *Lm*NOx has a molecular weight of approximately 50 kDa, containing a FAD cofactor and a cysteinyl redox center in the active site.[34] *Lm*NOx plays a vital role in replenishing NAD^+ necessary for glycolysis in homofermentative organisms,[35] enhancing their antioxidant defense mechanism in favor of the reduction of oxygen directly to H_2O rather than superoxide or H_2O_2.[35] This remarkable ability to facilitate direct four-electron reduction is attributed to the formation of a cysteine-sulfenic acid (Cys-SOH) intermediate at its nonflavin redox center in the active site for FAD regeneration (Scheme 1A).[36] Our goal is to engineer an enzyme-electrochemical couple based on the sequence of *Lm*NOx for NADH oxidation without dependence on molecular oxygen (Scheme 1B).

Electrochemical methods for cofactor regeneration have garnered significant interest as an alternative to chemical oxidation along with precise control of the electrode potential.[21,24,37−42] However, direct electron transfer (DET) between NADH in the active site of NOx and a solid electrode is challenging for two main reasons.[43] First, it is difficult to achieve an efficient electron transfer between the electrode surface and the active center in solution.[44] One possible way to alleviate this difficulty is to immobilize the enzyme on the electrode rather than rely on protein diffusion in the electrolyte solution. To this end, the biopolymer chitosan (CTS) provides a versatile platform for NOx immobilization since chitosan carries positive charges in solution, which facilitate interactions with the overall negatively charged NOx in addition to its low toxicity, biocompatibility, and film-forming capability. A further benefit is that the immobilized enzymes typically exhibit enhanced thermal stability and excellent reusability. Second, direct electron transfer between the enzyme and electrode often exhibits sluggish kinetics, irreversibility, and high activation energy and oxidation overpotential (reaching 1.1 V on carbon electrodes and 1.3 V on platinum electrodes at pH 7.0, respectively, vs SHE).[1,45−48] To overcome these difficulties, a wide range of electron transfer mediators have been developed in the past, including quinones,[25] phenoxazine,[49] phenothiazine,[50] and ferrocenes and their derivatives.[51] These small molecules have proven to be effective in infiltrating protein crevices and facilitating efficient shuttling between enzyme redox sites and electrode surfaces, thereby enhancing the catalytic oxidation of NADH by enzymes.

On the biosensor front for NADH detection, a wide range of electrochemical sensors have been developed, but they tend to have little substrate specificity; few devices have been designed based on enzymatic recognition of NADH.[44] Electrobiosensors offer significant advantages in substrate specificity over traditional detection methods, such as optical,[52] high-performance liquid chromatographic (HPLC),[53,54] electrophoresis,[55] and chemiluminescence.[56] We show that the engineered bioelectrocatalyst employing an electron transfer mediator can be an effective NADH biosensor that can operate under mild conditions with enhanced turnover efficiencies.

Herein, we present a bioelectrochemical approach for the oxidation of NADH catalyzed by *Lm*NOx immobilized on CTS-coated electrode. The primary objective is to replace the native cofactor regeneration half-reaction in the enzymatic cycle with an electrochemical process coupled with an *Lm*NOx mutant (Scheme 1). The essence of the present method involves electrochemical regeneration of the oxidized form of the FAD cofactor in the active site, eliminating the O_2-dependent second half-reaction of the native *Lm*NOx function and, thus, the need for bubbling air or pure oxygen in a biosynthetic reactor. To facilitate the electrochemical conversion at the electrode, ferrocene acetic acid (FcCA) is used as an electron transfer mediator. Furthermore, we show that this process can be used as a highly responsive electrochemical biosensor for NADH detection.

https://doi.org/10.1021/jacsau.4c00528
JACS Au 2024, 4, 3581−3592

EXPERIMENTAL SECTION

Electrolyte Buffer

The stability of NADH is highly dependent on electrolyte solvent and pH conditions.[57,58] Therefore, we examined a range of electrolyte buffer conditions for the present experiments. The variations in UV absorbance at 340 nm due to NADH were used to monitor the concentration change,[59] which are illustrated for three representative solvents and pH conditions in the Supporting Information (Figure S1). Among the solvents examined, we found that NADH has the greatest stability in the 1× PBS (phosphate-buffered saline) at pH 7.4, exhibiting just a 3% reduction in absorbance after 48 h of exposure to air. Other solvents presented greater losses of NADH under similar conditions with a reduction of NADH absorbance at 11.5 and 25.2%, respectively, for the 10× PBS (pH 7.4) and 50 mM MES (2-(*N*-morpholino)ethanesulfonic acid) buffer (pH 6.5). Consequently, we selected the 1× PBS as the electrolyte solution throughout this study except for cases specifically noted. Further details on pH effect for enzymes and buffer are given in the Supporting Information.

Ferrocene Carboxylic Acid (FcCA) as an Electron Transfer Mediator

Although the cofactor flavin adenine dinucleotide is noncovalently bound to the enzyme *Lm*NOx, it remains in the active site throughout the catalytic cycle of NADH oxidation.[34] The redox-active state FAD is regenerated within the *Lm*NOx active site in the second half of the catalytic cycle by oxidation of $FADH_2$ via the Cys-SOH intermediate from molecular oxygen, along with NADH oxidation and the production of water (Scheme 1A). As noted above, our goal is to replace the oxygen dependence in FAD regeneration during NOx catalysis by electrolysis without relying on bubbling air or oxygen in a biosynthetic system.[17−20] It turns out that direct electrochemical oxidation of $FADH_2$ to produce FAD is not efficient at the enzyme active site. Thus, we decided to employ a redox mediator to facilitate the electrochemical electron transfer process. Among the small-molecule electron mediators screened, such as benzoquinone, hydroquinone, and naphthalene-1,4-dione/diol, we found that ferrocene carboxylic acid (FcCA) is especially suited for this purpose. Despite its relatively high overpotential (ca. 0.5 V), FcCA was chosen because of its well-established reliability and stability in the whole enzymatic system. In contrast, other mediators showed an overpotential lower than that of FcCA, but many exhibited air instability and significant toxicity. For example, the redox peak of naphthalene-1,4-dione disappeared completely after exposure to air. The redox potential of FcCA is 0.99 V in 1× PBS at pH 7.4, higher than that of $FADH_2$ (0.23 V) (Figure S2).[60] Although the substrate NADH may appear to be directly oxidized by FcCA,[61] in practice, the mixed solution of NADH and FcCA is kinetically stable, without observable spontaneous reaction in 24 h.

The effect of FcCA on the electrochemical oxidation of NADH in the absence of the *Lm*NOx enzyme is depicted in Figure 1A, in which the overall potential is divided into four distinct reaction zones. First, a large potential for the direct electrolysis of NADH was observed, starting at 1.15 V (blue curve and cyan zone), consistent with previous studies.[62] When FcCA is introduced into the electrolyte solution (red curve), two changes are observed. First, the onset potential of NADH oxidation is noticeably reduced from 1.15 to 1.06 V, suggesting an electrocatalytic process by FcCA (purple zone). Second, within the range where FcCA is oxidized (red zone in Figure 1A), the peak height of the current density is increased, providing evidence for an indirect oxidation of NADH by FcCA. However, the observed change is rather small, reflecting a relatively slow or inefficient kinetic process. The findings in Figure 1A suggest that FcCA may be selected as the redox electron mediator for FAD electrocatalytic regeneration in the NOx enzyme, which indeed proved to be effective.

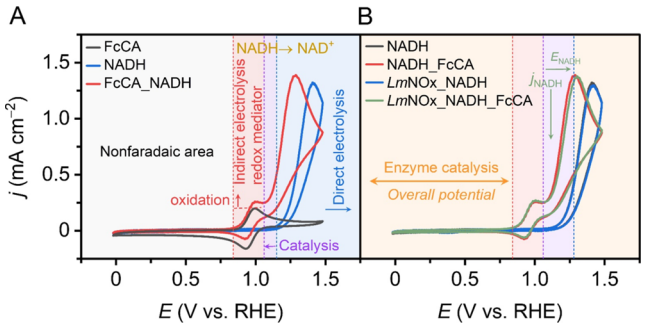

Figure 1. Electrocatalytic NADH oxidation performances of FcCA. Comparison of CV curves (A) without enzyme and (B) with free-*Lm*NOx at 25 μg (5 μL of a 5 mg/mL enzyme solution) in the electrolyte.

Effect of FcCA as a Mediator on NADH Oxidase Electrocatalysis

Shown in Figure 1B are the redox currents of NADH oxidation in the presence of *Lm*NOx enzyme with and without FcCA. All experiments were carried out using 1× PBS at pH 7.4 saturated by Ar gas, in which the overall *Lm*NOx catalytic cycle is essentially deactivated due to lacking O_2 to regenerate the FAD cofactor. Thus, any changes in the observed CV curves are due to NADH oxidation from electrocatalyzed FAD regeneration. However, we found that the CV curves are not much affected by the enzyme at low concentrations both with and without the electron transfer mediator FcCA (Figure S3).

Immobilization of NOx Enzyme on Glassy Carbon (GC) Electrode

The general procedure for NOx immobilization is illustrated in Scheme 2. Specifically, a solution of 0.5% fibrous polysaccharide chitosan (CTS) and *Lm*NOx solutions at a range of concentrations were prepared and stored at 4 °C. Then, the CTS and enzyme solutions were rapidly mixed at a 1:1 volume ratio under vigorous stirring until the mixture was homogeneous for approximately 20 min at 4 °C. The incubation period allowed the enzyme to be embedded in the CTS solution, becoming an integral part of the composite. Next, 5 μL of solution of the mixture was dropped onto the glassy carbon (GC) electrodes and dried at 4 °C overnight. Finally, to remove the loosely bound enzyme, the electrode was washed three times with fresh PBS, resulting in the *Lm*NOx/CTS@GC bioanode.

Characterization of Enzyme-Immobilized Electrode

Figure 2 shows the scanning electron microscopy (SEM) and confocal laser scanning microscopy (CLSM) images of *Lm*NOx immobilization. The pure enzyme powder forms sizable aggregates with a smooth surface (Figure 2A). For comparison, the *Lm*NOx solution exhibits a smaller size and a rough surface (Figure S4). Interestingly, a three-dimensional network is observed in the *Lm*NOx/CTS mixture (Figure 2B,C) in which the enzyme forms small block-like structures that intertwine and link together in the presence of CTS, generating a porous quasi-network structure that enhances the catalytic process. The uniformity of the enzyme distribution within the enzyme/CTS composites is shown in Figure 2D−I. The CLSM bright field images (Figure 2D,G) provide an overall perspective of the sample. In the CLSM fluorescence field, the enzyme sample shows a yellowish color under 445 nm laser excitation at 75 mW power and 30% intensity (Figure 2E,H). The integration of these images demonstrates a uniform and well-distributed enzyme presence throughout the CTS matrix, as shown in Figure 2F,I.

The morphology of the 0.25% CTS membrane was characterized by scanning electron microscopy (SEM). In Figure S5A,B, the CTS exhibits a two-dimensional (2D) plane structure. CV curves were employed to confirm the small-molecule inhibition characteristics of CTS. In Figure S5C, the incorporation of CTS at a mass fraction of 0.25% significantly hampers the catalytic oxidation performance of FcCA toward NADH. Specifically, the oxidation peak current of FcCA is lower than that of the bare GC electrode, while the onset potential for NADH electrocatalysis exhibits a slight increase, and the electrocatalytic current density is notably reduced. Despite CTS

https://doi.org/10.1021/jacsau.4c00528
JACS Au 2024, 4, 3581−3592

Scheme 2. Schematic Illustration of the Fabrication of *Lm*NOx/CTS@GC and the Redox Cycle of Ferrocene Acetic Acid-Mediated Electrocatalysis of NADH Oxidation and FAD Regeneration by NADH Oxidase (NOx)

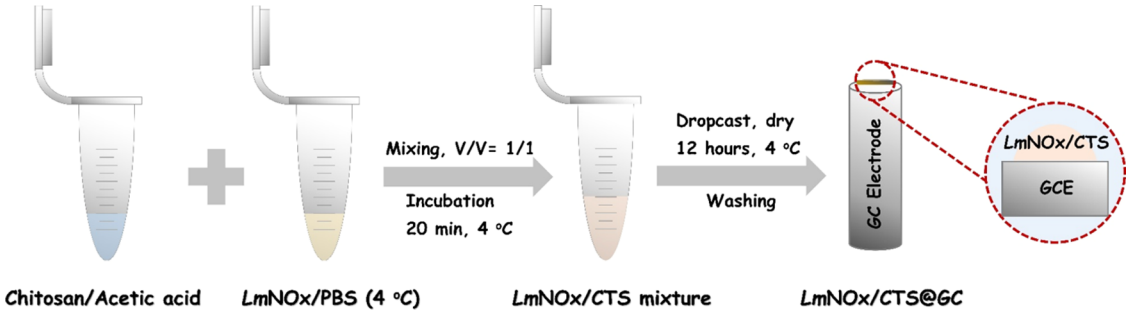

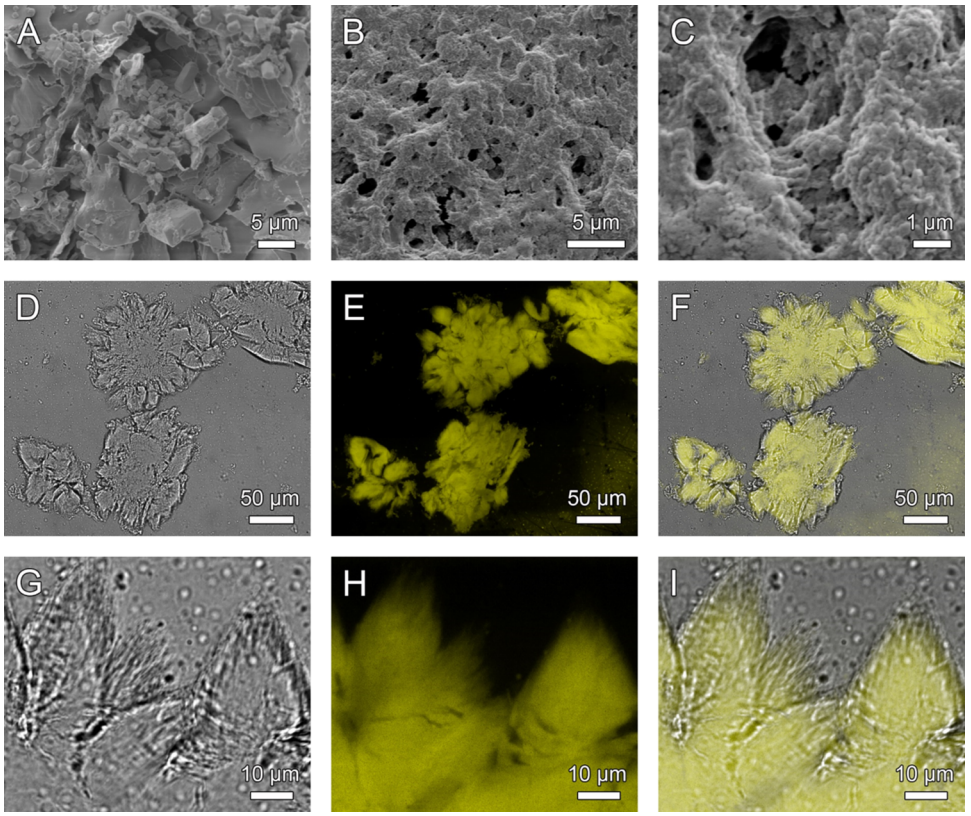

Figure 2. Morphology characterization. (A) SEM image of *Lm*NOx powder, (B, C) SEM images of *Lm*NOx/CTS, and (D–I) CLSM images of *Lm*NOx/CTS.

hindering the performance of FcCA, it still demonstrates a greater activity of catalytic oxidation in comparison with the system without the electron transfer mediator.

RESULTS AND DISCUSSION

Bioelectrocatalysis of NADH Oxidation by Wild-Type NADH Oxidase

The redox-active state of the cofactor FAD is regenerated through the second catalytic oxidation process by molecular oxygen in the active site of *Lm*NOx, along with the formation of water (Scheme 1).[36] Our goal is to replace oxygen dependence of NOx by electrocatalysis, thereby eliminating the need for molecular oxygen supply in the native enzyme cycle. However, it turns out that direct electrochemical oxidation of $FADH_2$ to produce FAD is not efficient in the enzyme active site, both in the presence or in the absence of a redox mediator such as FcCA. We hypothesized that the lack of NOx enzymatic activity on FAD regeneration via the electrolysis mediator is due to an inefficient diffusion of the enzyme to the electric double layer of the anode. To increase the efficiency of electrochemical oxidation in the *Lm*NOx active site, we immobilize the *Lm*NOx enzyme on a glassy carbon (GC) electrode using the fibrous polysaccharide chitosan (CTS) as an immobilization medium, which proved to be effective (Scheme 2).

Key findings are depicted in Figure 3, which compares the CV curves of the FcCA electrolyte solution using the NOx-immobilized electrode (*Lm*NOx/CTS@GC) both in the presence and absence of the enzyme substrate NADH. Specifically, in the absence of the substrate NADH, the enzymatic activity of NOx is discontinued such that Figure 3A (black curve) displays only the oxidation and reduction of the mediator FcCA/$FcCA^+$ with an oxidation current density peaked at 0.18 mA cm^{-2}. When the substrate NADH is added

https://doi.org/10.1021/jacsau.4c00528
JACS Au 2024, 4, 3581–3592

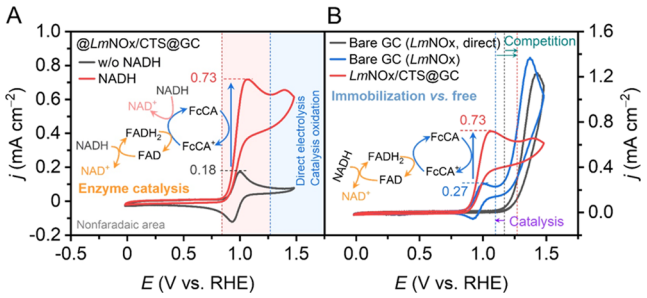

Figure 3. Bioelectrocatalytic NADH oxidation performances. (A) CV curves of *Lm*NOx/CTS@GC. (B) CV curves of bare GC and *Lm*NOx/CTS@GC in an enzyme-free electrolyte.

to the electrolyte solution, the CV curve (red) exhibits significant changes. First, the current peak height corresponding to the oxidation of FcCA is markedly enhanced by 4 times to 0.73 mA cm^{-2}. We attribute the observed increase in FcCA oxidation current intensity to the direct participation of the *Lm*NOx enzyme, in which the reactive form of the cofactor FAD in the catalytic cycle of NADH oxidation is regenerated by oxidation of $FADH_2$ via the mediator oxidant $FcCA^+$ at the electrode. Consequently, the reduced form of FcCA is reproduced from the coupled enzymatic action, enhancing the CV current relative to that of the background without the intervention of the NOx process.

Second, the reduction peak (black curve) of $FcCA^+$ disappears entirely in Figure 3A as the *Lm*NOx-catalyzed NADH oxidation takes place (red curve). This observation provides strong evidence that a significant portion of the oxidized $FcCA^+$ species generated directly by electrochemical oxidation is consumed through its active participation in the enzymatic cycle (Scheme 1B). Consequently, the electrochemical reduction of $FcCA^+$ is completely diminished. These findings demonstrate the successful realization of FAD cofactor regeneration in the enzyme active site by bioelectrocatalysis that is facilitated by the indirect electron transfer from $FADH_2$ to the anodic electrode via the mediator FcCA (see insert of Figure 3A).

We note that the overall observed enhancement in the current density corresponding to FcCA oxidation in Figure 3A potentially consists of two contributions: (1) directly from the enzymatic process in $FADH_2$ oxidation by $FcCA^+$ and (2) indirectly due to electrochemical oxidation of NADH aided via $FcCA^+$. To clarify the effect of mediator-assisted NADH oxidation at the enzyme-immobilized *Lm*NOx/CTS@GC electrode, we examined the oxidation currents of NADH using the bare GC electrode in a free (not immobilized) enzyme electrolyte solution that includes or excludes the electron transfer mediator FcCA. Figure 3B shows that without FcCA, the direct electrochemical oxidation of NADH is the only process observed (black curve), with no influence by the free enzyme in the electrolyte solution. On the other hand, a small increase in the FcCA oxidation peak height at 0.27 mA cm^{-2} (blue curve, Figure 3B) is recorded with the addition of FcCA mediator relative to the current height (0.18 mA cm^{-2}) for the process without NADH in the electrolyte solution (black curve in Figure 3A). Thus, there is indeed a small effect on FcCA oxidation accompanying electrochemical oxidation of NADH. In comparison with the oxidation reactions employing the *Lm*NOx-immobilized electrode, the CV peak corresponding to FcCA oxidation is markedly enhanced from 0.27 to 0.73 mA cm^{-2}, and this change can be entirely assigned to the enzymatic process. It is also instructive to notice that the amount of direct NADH electrooxidation on the enzyme-immobilized electrode at high voltage is significantly reduced, accompanied by a further delayed onset potential at 1.27 V (Figure 3B) relative to that of the direct NADH electrolysis process at 1.15 V. These observations reaffirm the mechanism of NADH oxidation by *Lm*NOx via bioelectrocatalysis of FAD cofactor regeneration.

The origin of the observed bioelectrocatalytic activity of NOx originates from enzyme immobilization on the GC electrode, since there is little enzymatic effect on the CV current of FcCA oxidation when the *Lm*NOx enzyme is simply dissolved in the electrolyte solution. The CTS network structures shown in the SEM images (Figure 2) provide a matrix that confines the enzyme in close contact with the electrode, where the mediator oxidant is generated for efficient electron transfer from $FADH_2$ in the enzyme active site. Thus, the overall effect is that the anodic electrode indirectly contributes to the oxidation of $FADH_2$ by the enzymatic conversion of $FcCA^+$ to FcCA, resulting in the disappearance of its reductive peak and an increase in the oxidative peak. The increased onset potential for NADH electrocatalysis is also an indication that the local concentration of NADH around the electrode surface is lowered because of enzymatic binding. This is mirrored by the significant reduction of direct NADH oxidation current density at high voltages, using the NOx-immobilized electrode, in comparison with the bare GC electrode. These results provide further compelling evidence for the successful fabrication of an electrochemically assisted *Lm*NOx biocatalytic system (Scheme 2), enabling oxygen-independent and continuous catalytic oxidation of NADH.

We also systematically optimized the CTS concentration and the amount of immobilized *Lm*NOx on electrode preparation. The impact of CTS concentration is illustrated in Figure S6A at weight fractions of 0.125, 0.25, and 0.5% with a constant *Lm*NOx load of 25 μg. Comparing the changes in CV curves, we conclude that a CTS concentration of 0.25% has the optimal performance in the present construct. This choice can be explained by two competitive factors, from the perspectives of binder and inhibitor. First, to ensure the secure immobilization of the enzyme on the GC electrode, it is essential that the CTS binder possesses adequate viscosity to prevent the enzyme from detaching. Second, CTS tends to inhibit electrolysis of small molecules (Figure S5C), and a high CTS concentration is also not ideal. Consequently, the optimal 0.25% CTS mass fraction is a result of these two competing factors.

The optimal amount of enzyme loading in the immobilization process was investigated on a series of experiments using 25, 50, 75, and 100 μg of the NOx enzyme at a fixed 0.25% CTS concentration. We found that a higher enzyme load of *Lm*NOx at 75 μg exhibits the best performance (Figure S6). First, CTS was dissolved in acetic acid at pH 5.0, resulting in the inactivation of the vast majority of the enzyme catalyst. Consequently, not all enzymes can participate in the subsequent catalytic reactions. Second, within a certain range, the increase in loading mass is directly proportional to the rise in the oxidation current density of FcCA. However, the oxidation current cannot continue to increase indefinitely due to the limitations imposed by the surface area of the GC electrode. This is attributed to the increased thickness of the *Lm*NOx/CTS layer on the GC electrode, which decreases the

https://doi.org/10.1021/jacsau.4c00528
JACS Au 2024, 4, 3581−3592

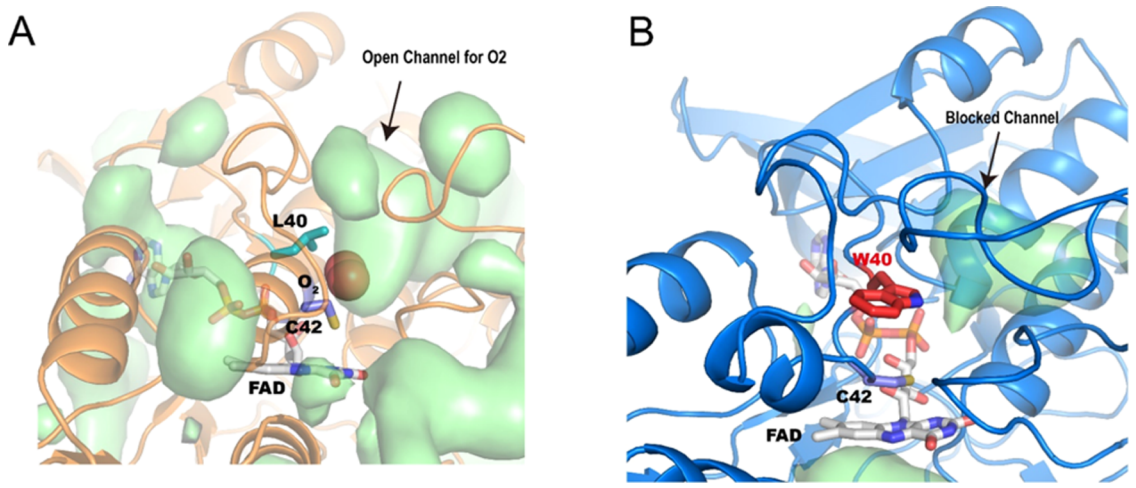

Figure 4. Comparison of cavity at a frequency contour of 0.3 for (A) *Lm*NOx wild type and (B) L40W, highlighting the blocked of the O_2 channel in the latter.

diffusion of FcCA to and from the electrode surface. The linear dependence of I_{pa} and I_{pc} as a function of square root of the scan rate ($\nu^{1/2}$) further showed the diffusion-controlled process on the electrode surface as shown in Figure S7. In summary, the optimal conditions for the mass fraction of CTS and enzyme amount in *Lm*NOx/CTS@GC were determined to be 0.25% and 75 μg, respectively.

Design of an O_2-Independent NOx for Electrochemical Oxidation of NADH

Wild-type *Lm*NOx catalyzes NADH oxidation by molecular oxygen, which also regenerates the FAD cofactor in the active site. To ensure that the oxidation of $FADH_2$ is exclusively electrochemical, all experiments in the previous section were carried out strictly in a sealed H-type Nafion 117 membrane electrolysis cell saturated with argon gas. This is quite effective, evidenced by a net loss of NADH absorbance at 340 nm by only 0.3% in the *Lm*NOx/CTS@GC cell after 12 h, compared to a spontaneous reduction of more than 95% when it is exposed to air (Figure S8). Nevertheless, to mitigate the potential influence of dissolved oxygen in bioelectrocatalysis under atmosphere rather than argon gas, which can also be used as a highly sensitive NADH electrochemical biosensor, we carried out a series of molecular dynamics (MD) simulations, which allowed us to design and engineer a mutant NADH oxidase for use in bioelectrocatalysis that is independent of molecular oxygen. In recent decades, research groups including those of Léger's and Stripp's have conducted a series of studies on improving O_2-tolerance by hydrogenases through protein engineering in key residue site, providing a clear theoretical understanding of tolerance changes.[63−72]

An obvious target for mutation is the catalytic residue Cys42, which is oxidized to a sulfenic acid intermediate by the hydrogen peroxyl adduct of $FADH_2$; the latter is produced in the first half of the *Lm*NOx reaction (Scheme 1A). In turn, the Cys42-SOH intermediate serves as the oxidizing agent in the second half of the enzymatic action, giving rise to two molecules of NAD^+ and one water (overall involving 4 e^- and 4 H^+ transfer) in the full enzyme cycle. However, a direct mutation of Cys42, for example to Ser42, which terminates the second enzymatic oxidation reaction is of no practical use since hydrogen peroxide is produced, rather than water, which inactivates enzyme activities if not removed. Consequently, we hypothesized that a coupled action of inhibition in the enzymatic O_2-binding and Cys42 mutation in the active site will be sufficient to eliminate the competition of the enzymatic O_2 pathway in electrocatalysis.

We first conducted molecular dynamics (MD) simulations of the wild-type *Lm*NOx, and we analyzed the cavity opening dynamics along a conduit for O_2 binding during a 500 ns MD trajectory. Figure 4A displays persistent cavities in the protein at frequencies greater than 60% along the entire trajectory, based on which a pathway for oxygen binding in the active site can be identified, leading to the exterior of the enzyme. It can be seen that Leu40, which is away from the active site and not directly involved in the NOx oxidation−reduction cycle, is directly coupled to oxygen binding, playing the role of channel gating for oxygen passage. We then carried out an additional series of molecular dynamics simulations of the Leu40 mutants and found that the opening frequency of the oxygen channel in the Leu40Trp (L40W) mutant is reduced to less than 20% (Figure 4B), suggesting that the bulky indole side chain of Trp40 can potentially inhibit the diffusion of O_2 to the active center.

Experimentally, the L40W mutant was successfully expressed in *Escherichia coli* BL21(DE3) and characterized as shown in Figure S9. The molecular weights of the wild-type and mutant enzymes in this study were approximately 102.5 kDa. In the enzymatic activity assay, the catalytic rate (k_{cat}) of L40W is reduced from 159 s^{-1} for the wild-type *Lm*NOx to 30 s^{-1} at pH 7.4 (Figure S10 and Table S1). Although the enzyme activities are not fully deactivated, suggesting that molecular oxygen can still diffuse into the active site, the markedly reduced catalytic rate in the L40W mutant demonstrates a successful selection of the mutation site.

We next examine the coupled effect of both Leu40 and Cys42 mutations.[35,36] We carried out a set of saturation mutagenesis experiments at Cys42 based on the L40W variant and generated a total of 19 double mutants (Table S2). Two mutants, Leu40Trp/Cys42Ala (L40W/C42A) and Leu40Trp/Cys42Gly (L40W/C42G), were purified as yellow powders, indicating successful incorporation of the FAD cofactor in the active site (Figure S11). One of the constructs, the L40W/C42A double mutant, retains some enzyme activities where hydrogen peroxide H_2O_2 is produced instead of water (Figure S12). However, the catalytic reactivity (k_{cat}) is significantly

https://doi.org/10.1021/jacsau.4c00528
JACS Au 2024, 4, 3581−3592

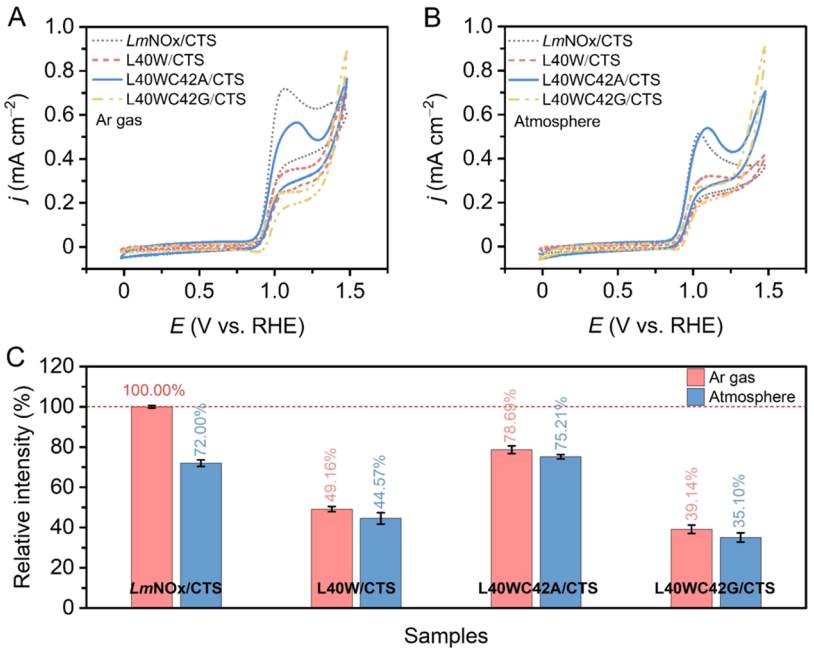

Figure 5. Bioelectrocatalytic NADH oxidation performances. CV curves of *Lm*NOx/CTS@GC and the mutant samples (A) in Ar gas-saturated electrolyte and (B) in the atmosphere. (C) Comparison of these catalysts regarding the peak current density under both Ar gas and atmosphere.

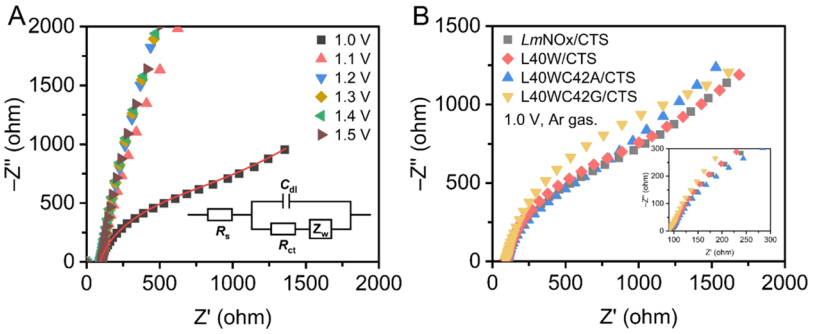

Figure 6. Nyquist plots for the ferrocene acetic acid-mediated electrocatalytic oxidation of NADH using an enzyme-immobilized electrode. (A) Wild-type enzyme *Lm*NOx at different electrode potentials and (B) L40W, L40W/C42A, and L40W/C42G mutants at 1.0 V potential.

decreased to just about 5% of that of the wild-type enzyme. Additional details are given in the Supporting Information.

Before we proceeded to electrocatalysis, the physicochemical properties of the mutant enzymes were further characterized (Figures S13−S19). Specifically, all mutants show an optimal pH of 6.5 that is the same as that of the wild-type *Lm*NOx enzyme (Figure S13). Under the experimental conditions of 1× PBS at pH 7.4, the L40W/C42G double mutant has the least specific activity (SA)—a measure of the turnover number (k_{cat}) in units of enzyme weight—toward NADH oxidation at about 3.0 U mg^{-1} (U = 1 μmol min^{-1}), which may be compared with that of 107.7 U mg^{-1} for the wild-type enzyme. We found that all enzymes, including the wild-type, are unstable at pH below 5.0 after 4 h, retaining only about 15% of the initial SA, whereas the double mutants become inactive below pH 6.0 (Figure S14). In contrast, all enzymes exhibited stable SA at pH 7.4, which coincided with the pH of the 1× PBS electrolyte buffer used in this work. In addition, different metal ions, EDTA, and Triton X100 all impact the catalytic activity in varying degrees for the four (wild-type and three mutants) enzymes, with the L40W/C42A double mutant showing the least dependence (Figure S15). Therefore, a mild pH of 7.4 was chosen, along with metal-free reaction conditions for all experiments in this study. Furthermore, since the *Lm*NOx is a typical flavoprotein oxidase (Figure S11), the impact of exogenous flavin cofactor on SA was also investigated to confirm that the flavin cofactor is not covalently bound to the native enzyme (Figure S16), as observed in other oxidases.[73] In addition, circular dichroism (CD), differential scanning fluorimetry (DSF), and dynamic light scattering (DLS) results were also studied (Figures S17−S19 and Tables S3−S4), further details can be found in the Supporting Information.

The bioelectrocatalytic activities of the three mutant enzymes immobilized on GC electrodes are compared in Figure 5 with that of the wild-type *Lm*NOx under conditions both saturated with Ar gas (Figure 5A) and exposed to the atmosphere (Figure 5B). Anaerobically, the intrinsic activity of cofactor FAD regeneration corresponding to the second half of the enzyme cycle is suppressed. The most striking finding in Figure 5A,B is that the oxidation current peaks of the FcCA mediator, recorded using electrodes intercalated with mutant enzymes, show little variance between conditions exposed to air and argon gas (Figure 5C). This is in sharp contrast to that

https://doi.org/10.1021/jacsau.4c00528
JACS Au 2024, 4, 3581−3592

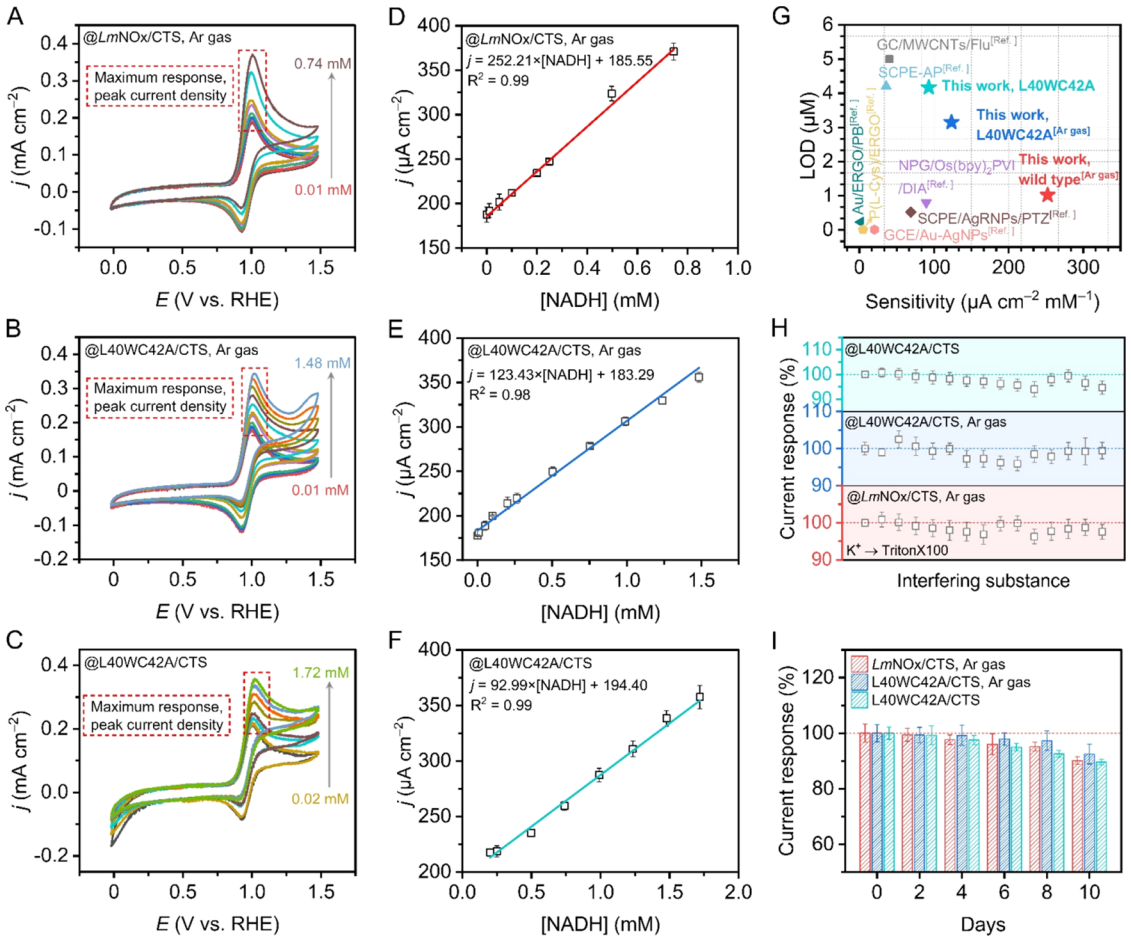

Figure 7. NADH electrochemical biosensor performances. (A−C) CV curves of *Lm*NOx/CTS@GC and L40WC42A/CTS@GC with various concentrations of NADH in Ar gas-saturated or oxygen-containing electrolyte and (D−F) the corresponding linear relationship of two samples between the oxidation peak current densities and the concentrations of NADH. (G) NADH detection performance comparison of our work with reported works. (H) Interference immunity assay. (I) Stability assay.

of the wild-type enzyme electrode (gray curves), which shows a significant reduction when the electrolyte solution is exposed to air (Figure 5C). The observations suggest that competition against electrocatalysis by native enzyme activity following the oxygen pathway has been effectively suppressed in all three mutants (L40W, L40W/C42A, and L40W/C42G). However, all three mutants show reduced electrocatalytic efficiencies, measured by the oxidation level of the redox mediator FcCA, ranging from 79% in L40W/C42A to 39% in L40W/C42G relative to the wild-type enzyme (Figure 5C). Of the mutants, the L40W/C42A double mutant exhibits the most favorable resurrection results among the three mutants with a maximum current density of 79% compared to the wild type in the Ar gas-saturated electrolyte. The effect of oxygen in air on electrocatalysis in the L40W/C42A-immobilized electrode is relatively small, with a reduction of only 3.5% relative to that under anaerobic conditions.

Figure 6 reports the electrocatalytic kinetic behavior at the enzyme-immobilized electrodes using electrochemical impedance spectroscopy (EIS) measurements.[74] Figure 6A displays the Nyquist plots of wild-type *Lm*NOx/CTS@GC at different potentials, while Figure 6B depicts results from the three mutant enzymes under a constant voltage of 1.0 V. The insert of Figure 6A shows an equivalent electrical circuit used to model the EIS data, in which R_s is the overall series resistance, C_{dl} is the double-layer capacitance characteristic of the enzyme electrode and electrolyte interface, Z_w is the Warburg impedance associated with ion diffusion, and R_{ct} is the charge-transfer resistance related to the NADH electrooxidation process. We found that the Nyquist plots exhibit obviously different R_{ct} values for *Lm*NOx/CTS@GC at various potentials. Remarkably, the potential at 1.0 V shows the smallest semicircle, indicating the lowest charge-transfer resistance at the catalyst/electrolyte interface, consistent with its superior catalytic activity. This result further confirms the mediating role of FcCA, highlighting that the entire system is most easily driven at the maximum oxidation potential of FcCA, which is distinctively smaller than that of direct oxidation of NADH at the electrode. Figure 6B illustrates the Nyquist plots for the mutants, which reveal the R_{ct} values for the mutant catalysts at a potential of 1.0 V. Among the three mutants, the L40W/C42A double mutation gives the smallest semicircle, indicating the lowest charge-transfer resistance at the catalyst/electrolyte interface, in line with its superior catalytic activity.

In summary, the function of NADH oxidase within the oxygen pathway was inhibited through a computation-aided rational design approach, concurrently achieving successful electrochemical resurrection. This forms the experimental basis for the development of a highly responsive NADH electrochemical biosensor with a low detection limit and a wide detection range.

https://doi.org/10.1021/jacsau.4c00528
JACS Au 2024, 4, 3581−3592

NADH Electrochemical Biosensor

While the bioelectrocatalytic process for NADH oxidation mediated by ferrocene acetic acid (FcCA) using mutant NOx-immobilized electrodes can be coupled to a NAD-dependent oxidase such as alcohol dehydrogenase in a biosynthetic cycle, the successful design of an oxygen-independent NOx enzyme can be used as an NADH electrochemical biosensor. In this section, we show that this device is highly responsive with a low detection limit and wide detection ranges. We compare the responsiveness for NADH using the wild-type *Lm*NOx and the L40W/C42A mutant enzymes in the potential range of −0.7 to 0.8 V (vs SCE). Subsequently, quantitative analysis was performed by correlating the current response signals with various NADH concentrations, establishing a linear relationship.

The CV response to various NADH concentrations using the wild-type *Lm*NOx-immobilized electrode is shown in Figure 7A. With the change in the current density of FcCA oxidation peak as reference, a strong linear correlation was obtained over the range of 10−740 μM (Figure 7D), characterized by the linear relationship j (μA cm^{-2}) = 252.21 × [NADH] (mM) + 1.02 (R^2 = 0.99). Here, j denotes the change in the oxidation peak current density of FcCA, [NADH] represents the NADH concentration, and R^2 is the Pearson correlation coefficient. The sensitivity of this system, defined by the slope, is 252.21 μA cm^{-2} mM^{-1}. The limit of detection (LOD) is defined as LOD = 3S/N, where S is the standard deviation of 10 consecutive blank samples and N is the sensitivity. In all, the LOD for the bioelectric sensor using the wild-type *Lm*NOx is determined to be 1.02 μM. Illustrated in Figure 7B,E is the NADH electrochemical biosensor constructed with the L40W/C42A mutant, showing a linear range of 10−1480 μM, with a sensitivity of 123.43 μA cm^{-2} mM^{-1} and an LOD of 4.17 μM.

The performances of the two bioelectric sensing devices were also assessed under conditions exposed to air (Figure S20). However, a linear relationship cannot be obtained over the same range of NADH concentrations using the wild-type *Lm*NOx. In contrast, a well-defined current response CV curve with a linear relationship can be constructed with the L40W/C42A mutant (Figure 7C,F). The different kinetic behaviors between wild-type and mutant *Lm*NOx under the atmosphere are consistent with the design goal of inactivation of the second-half, oxygen-dependent pathway that regenerates the enzyme cofactor FAD in the active site. Although sensitivity and LOD are slightly decreased in the mutant system, a wider detection range was achieved. This characteristic makes it applicable for different test situations, and the mutant biosensor could reflect the true NADH level as accurately as possible. In Figure 7G, we compare the NADH detection performance LOD of our work in terms of LOD with data reported in the literature, most of which employ traditional metal-alloy or glassy carbon electrodes, revealing that the present bioelectrocatalytic device has a performance comparable to that of the best detection limits in the literature (additional data can be found in Table S5).

To illustrate the capability of substrate specificity, various interfering substances were introduced into the system to assess the anti-interference selectivity of the present two electrochemical biosensors (wild-type NOx and the L40W/C42A mutant). We found that both wild-type and mutant biosensors have remarkable ability against interference from other substances when the sample is exposed to a majority of interfering substances (Figure 7H). Additionally, the biosensors also possess excellent stability lasting for 10 days (Figure 7I). In conclusion, both pre- and postmutation states offer distinct advantages and are suitable for NADH concentration detection in diverse scenarios.

CONCLUSIONS

The flavoprotein NADH oxidase from *L. mesenteroides* (*Lm*NOx) catalyzes the oxidation of NADH to NAD$^+$ by molecular oxygen. Coupled with dehydrogenase enzymes that utilize NAD$^+$(NADP$^+$) as cofactors, NADH oxidases can be used to regenerate the oxidized cofactors in situ for biocatalytic processes, such as alcohol oxidation to carbonyl compounds. However, a major limitation is the need to supply oxygen through bubbling air or pure oxygen in a biosynthesis reactor, which tends to reduce enzyme stability in practice. In this study, a coupled electrochemical and enzymatic process for NADH oxidation is successfully achieved in which the oxygen-dependent activities of wild-type NADH oxidase are replaced by electrochemical oxidation of the reduced $FADH_2$ cofactor in the active site. This is accomplished through a combination of enzyme immobilization on the electrode and electrochemical redox mediation via ferrocene carboxylic acid (FcCA). The present bioelectrocatalysis system can be operated both under anaerobic conditions saturated with argon gas or under atmospheric conditions; however, the latter is complicated by competition between the native enzyme and coupled electrocatalytic processes.

To minimize the impact of dissolved oxygen exposed to air, we designed several mutants of *Lm*NOx, guided by molecular dynamics simulations with the aim to block the oxygen passage into the active site and remove the sulfenic acid site in the second half of the native NOx cycle. The double mutations at the Leu40 and Cys42 sites proved to be effective, significantly reducing or eliminating NADH oxidation activities in solution due to a lack of cofactor regeneration. Importantly, the engineered enzymes, coupled with electrolytic oxidation of FcCA to facilitate FAD cofactor regeneration in the active site, are catalytically active toward the conversion of NADH to NAD$^+$. The engineered bioelectrocatalytic system has an activity as high as 79% of the wild-type enzyme. Finally, two highly responsive electrochemical biosensors for NADH detection have been developed, exhibiting a broad detection range and low detection limit. The present results demonstrate that a native enzymatic cycle can be engineered to meet specific needs, in which the altered path of the enzymatic process may be replaced by an external electrochemical reaction. Furthermore, we found that efficient electron transfer between a cofactor in the enzyme active site and an electrode can be achieved via a redox mediator, in this case, FcCA. It would be of interest to engineer enzymes or processes that can be used for the direct electron transfer (DET) between the active site and electrode.

ASSOCIATED CONTENT

Supporting Information

The Supporting Information is available free of charge at https://pubs.acs.org/doi/10.1021/jacsau.4c00528.

Summary of the experimental procedures, computational methods, and additional details (PDF)

https://doi.org/10.1021/jacsau.4c00528
JACS Au 2024, 4, 3581−3592

AUTHOR INFORMATION

Corresponding Authors

Jing Yuan − *Institute of Systems and Physical Biology, Shenzhen Bay Laboratory, Shenzhen 518055, China;* orcid.org/0009-0007-0849-0613; Email: yuanj@szbl.ac.cn

Shihe Yang − *School of Advanced Materials, Peking University Shenzhen Graduate School, Shenzhen 518055, China; Institute of Biomedical Engineering, Shenzhen Bay Laboratory, Shenzhen 518055, China;* orcid.org/0000-0002-6469-8415; Email: chsyang@pku.edu.cn

Jiali Gao − *School of Chemical Biology and Biotechnology, Peking University Shenzhen Graduate School, Shenzhen 518055, China; Institute of Systems and Physical Biology, Shenzhen Bay Laboratory, Shenzhen 518055, China; Department of Chemistry and Supercomputing Institute, University of Minnesota, Minneapolis, Minnesota 55455, United States;* orcid.org/0000-0003-0106-7154; Email: gao@jialigao.org

Authors

Mengjie Hou − *School of Chemical Biology and Biotechnology, Peking University Shenzhen Graduate School, Shenzhen 518055, China; Institute of Systems and Physical Biology, Shenzhen Bay Laboratory, Shenzhen 518055, China;* orcid.org/0000-0002-4403-7118

Xinyu Dong − *Institute of Systems and Physical Biology, Shenzhen Bay Laboratory, Shenzhen 518055, China*

Yingjie Wang − *Institute of Systems and Physical Biology, Shenzhen Bay Laboratory, Shenzhen 518055, China;* orcid.org/0000-0001-9800-8163

Complete contact information is available at: https://pubs.acs.org/10.1021/jacsau.4c00528

Author Contributions

CRediT: **Mengjie Hou** conceptualization, data curation, formal analysis, methodology, writing-original draft; **Jing Yuan** conceptualization, formal analysis, investigation, methodology, writing-review & editing; **Xinyu Dong** data curation, resources; **Yingjie Wang** data curation, software; **Shihe Yang** conceptualization, formal analysis, writing-review & editing; **Jiali Gao** conceptualization, formal analysis, resources, writing-review & editing.

Notes

The authors declare no competing financial interest.

ACKNOWLEDGMENTS

This work was supported by Shenzhen Municipal Science and Technology Innovation Commission (KQTD2017-0330155106581) and the Computational facilities of Shenzhen Bay Laboratory. M.H. acknowledges Cheng Zhou and Mengsi Sun of the Biochemistry Core Facilities at Shenzhen Bay Laboratory for assistance with the CD and DSF experiment.

REFERENCES

(1) Han, S.; Du, T.; Jiang, H.; Wang, X. Synergistic Effect of Pyrroloquinoline Quinone and Graphene Nano-Interface for Facile Fabrication of Sensitive NADH Biosensor. *Biosens. Bioelectron.* **2017**, *89* (1), 422−429.

(2) Tan, X.; Nielsen, J. The Integration of Bio-Catalysis and Electrocatalysis to Produce Fuels and Chemicals from Carbon Dioxide. *Chem. Soc. Rev.* **2022**, *51* (11), 4763−4785.

(3) Liu, Y.; Landick, R.; Raman, S. A Regulatory NADH/NAD^+ Redox Biosensor for Bacteria. *ACS Synth. Biol.* **2019**, *8* (2), 264−273.

(4) Eto, K.; Tsubamoto, Y.; Terauchi, Y.; Sugiyama, T.; Kishimoto, T.; Takahashi, N.; Yamauchi, N.; Kubota, N.; Murayama, S.; Aizawa, T.; Akanuma, Y.; Aizawa, S.; Kasai, H.; Yazaki, Y.; Kadowaki, T. Role of NADH Shuttle System in Glucose-Induced Activation of Mitochondrial Metabolism and Insulin Secretion. *Science* **1999**, *283* (5404), 981−985.

(5) Santidrian, A. F.; Matsuno-Yagi, A.; Ritland, M.; Seo, B. B.; LeBoeuf, S. E.; Gay, L. J.; Yagi, T.; Felding-Habermann, B. Mitochondrial Complex I Activity and NAD^+/NADH Balance Regulate Breast Cancer Progression. *J. Clin. Invest.* **2013**, *123* (3), 1068−1081.

(6) Labib, M.; Sargent, E. H.; Kelley, S. O. Electrochemical Methods for the Analysis of Clinically Relevant Biomolecules. *Chem. Rev.* **2016**, *116* (16), 9001−9090.

(7) Sharma, R.; Reinstadler, B.; Engelstad, K.; Skinner, O. S.; Stackowitz, E.; Haller, R. G.; Clish, C. B.; Pierce, K.; Walker, M. A.; Fryer, R.; Oglesbee, D.; Mao, X.; Shungu, D. C.; Khatri, A.; Hirano, M.; Vivo, D. C. D.; Mootha, V. K. Circulating Markers of NADH-Reductive Stress Correlate with Mitochondrial Disease Severity. *J. Clin. Invest.* **2021**, *131* (2), No. e136055.

(8) Sha, F.; Zheng, Y.; Chen, J.; Chen, K.; Cao, F.; Yan, M.; Ouyang, P. D-Tagatose Manufacture through Bio-Oxidation of Galactitol Derived from Waste Xylose Mother Liquor. *Green Chem.* **2018**, *20* (10), 2382−2391.

(9) Teymourian, H.; Salimi, A.; Hallaj, R. Low Potential Detection of NADH Based on Fe_3O_4 Nanoparticles/Multiwalled Carbon Nanotubes Composite: Fabrication of Integrated Dehydrogenase-Based Lactate Biosensor. *Biosens. Bioelectron.* **2012**, *33* (1), 60−68.

(10) Jaegfeldt, H.; Kuwana, T.; Johansson, G. Electrochemical Stability of Catechols with a Pyrene Side Chain Strongly Adsorbed on Graphite Electrodes for Catalytic Oxidation of Dihydronicotinamide Adenine Dinucleotide. *J. Am. Chem. Soc.* **1983**, *105* (7), 1805−1814.

(11) del Barrio, M.; Rana, M.; Vilatela, J. J.; Lorenzo, E.; De Lacey, A. L.; Pita, M. Photoelectrocatalytic Detection of NADH on N-Type Silicon Semiconductors Facilitated by Carbon Nanotube Fibers. *Electrochim. Acta* **2021**, *377*, 138071−138079.

(12) Wilson, T. A.; Musameh, M.; Kyratzis, I. L.; Zhang, J.; Bond, A. M.; Hearn, M. T. W. Enhanced NADH Oxidation Using Polytyramine/Carbon Nanotube Modified Electrodes for Ethanol Biosensing. *Electroanalysis* **2017**, *29* (8), 1985−1993.

(13) Liu, Z. X.; Gao, Y. D.; Yang, L. C. Biocatalytic Hydrogen-Borrowing Cascade in Organic Synthesis. *JACS Au* **2024**, *4* (3), 877−892.

(14) Gao, X.; Lu, R.; Zhou, Y.; Lin, L.; Ji, X.-J. One-Pot Multi-Enzyme Cascade Synthesis of Bifunctional Compounds from Vegetable Oils. *Synth. Biol. Eng.* **2024**, *2* (1), 10004.

(15) Yuan, M.; Kummer, M. J.; Milton, R. D.; Quah, T.; Minteer, S. D. Efficient NADH Regeneration by a Redox Polymer-Immobilized Enzymatic System. *ACS Catal.* **2019**, *9* (6), 5486−5495.

(16) Partipilo, M.; Claassens, N. J.; Slotboom, D. J. A Hitchhiker's Guide to Supplying Enzymatic Reducing Power into Synthetic Cells. *ACS Synth. Biol.* **2023**, *12* (4), 947−962.

(17) Mital, S.; Christie, G.; Dikicioglu, D. Recombinant Expression of Insoluble Enzymes in *Escherichia coli*: A Systematic Review of Experimental Design and Its Manufacturing Implications. *Microb. Cell Fact.* **2021**, *20* (1), 208.

(18) Wang, J.; Woodley, J. M. In Situ Cofactor Regeneration Using NAD(P)H Oxidase: Enzyme Stability in a Bubble Column. *ChemCatChem* **2022**, *14* (15), No. e202200255.

(19) Anderson, S. R.; Bommarius, B. R.; Woodley, J. M.; Bommarius, A. S. Sparged but Not Stirred: Rapid, Adh-NADH Oxidase Catalyzed Deracemization of Alcohols in a Bubble Column. *Chem. Eng. J.* **2021**, *417*, 127909−127915.

(20) Wang, J.; Erdem, E.; Woodley, J. M. Effect of Nitrogen, Air, and Oxygen on the Kinetic Stability of NAD(P)H Oxidase Exposed to a Gas-Liquid Interface. *Org. Process Res. Dev.* **2023**, *27* (6), 1111−1121.

(21) Wang, X.; Saba, T.; Yiu, H.; Howe, R. F.; Anderson, J. A.; Shi, J. Cofactor NAD(P)H Regeneration Inspired by Heterogeneous Pathways. *Chem* **2017**, *2* (5), 621−654.
(22) Jayathilake, B. S.; Bhattacharya, S.; Vaidehi, N.; Narayanan, S. R. Efficient and Selective Electrochemically Driven Enzyme-Catalyzed Reduction of Carbon Dioxide to Formate Using Formate Dehydrogenase and an Artificial Cofactor. *Acc. Chem. Res.* **2019**, *52* (3), 676−685.
(23) Sokol, K. P.; Robinson, W. E.; Oliveira, A. R.; Warnan, J.; Nowaczyk, M. M.; Ruff, A.; Pereira, I. A. C.; Reisner, E. Photoreduction of CO_2 with a Formate Dehydrogenase Driven by Photosystem II Using a Semi-Artificial Z-Scheme Architecture. *J. Am. Chem. Soc.* **2018**, *140* (48), 16418−16422.
(24) Tsujimura, S. From Fundamentals to Applications of Bioelectrocatalysis: Bioelectrocatalytic Reactions of FAD-dependent Glucose Dehydrogenase and Bilirubin Oxidase. *Biosci. Biotechnol. Biochem.* **2019**, *83* (1), 39−48.
(25) Babanova, S.; Matanovic, I.; Chavez, M. S.; Atanassov, P. Role of Quinones in Electron Transfer of PQQ-Glucose Dehydrogenase Anodes-Mediation or Orientation Effect. *J. Am. Chem. Soc.* **2015**, *137* (24), 7754−7762.
(26) Liu, X.; Li, J.; Zitolo, A.; Gao, M.; Jiang, J.; Geng, X.; Xie, Q.; Wu, D.; Zheng, H.; Cai, X.; Lu, J.; Jaouen, F.; Li, R. Doped Graphene to Mimic the Bacterial NADH Oxidase for One-Step NAD^+ Supplementation in Mammals. *J. Am. Chem. Soc.* **2023**, *145* (5), 3108−3120.
(27) Makarov, M. V.; Hayat, F.; Graves, B.; Sonavane, M.; Salter, E. A.; Wierzbicki, A.; Gassman, N. R.; Migaud, M. E. Chemical and Biochemical Reactivity of the Reduced Forms of Nicotinamide Riboside. *ACS Chem. Biol.* **2021**, *16* (4), 604−614.
(28) Boecker, M.; Micheel, M.; Mengele, A. K.; Neumann, C.; Herberger, T.; D'Alvise, T. M.; Liu, B.; Undisz, A.; Rau, S.; Turchanin, A.; Synatschke, C. V.; Wächtler, M.; Weil, T. Rhodium-Complex-Functionalized and Polydopamine-coated CdSe@CdS Nanorods for Photocatalytic NAD^+ Reduction. *ACS Appl. Nano Mater.* **2021**, *4* (12), 12913−12919.
(29) Dong, F.; Chen, H.; Malapit, C. A.; Prater, M. B.; Li, M.; Yuan, M.; Lim, K.; Minteer, S. D. Biphasic Bioelectrocatalytic Synthesis of Chiral B-Hydroxy Nitriles. *J. Am. Chem. Soc.* **2020**, *142* (18), 8374−8382.
(30) Zhang, J. D.; Cui, Z. M.; Fan, X. J.; Wu, H. L.; Chang, H. H. Cloning and Characterization of Two Distinct Water-Forming NADH Oxidases from Lactobacillus Pentosus for the Regeneration of NAD. *Bioprocess Biosyst. Eng.* **2016**, *39* (4), 603−611.
(31) Liu, S.; Wang, Z.; Wang, L.; Zhang, S.; Sun, Y. Self-Sufficient Heterogeneous Biocatalysis Systems Based on NAD(P) Recycling: New Perspectives on Construction. *Catal. Rev.* **2023**, 1−43.
(32) Nowak, C.; Beer, B.; Pick, A.; Roth, T.; Lommes, P.; Sieber, V. A Water-Forming NADH Oxidase from Lactobacillus Pentosus Suitable for the Regeneration of Synthetic Biomimetic Cofactors. *Front. Microbiol.* **2015**, *6*, 957.
(33) Li, F. L.; Shi, Y.; Zhang, J. X.; Gao, J.; Zhang, Y. W. Cloning, Expression, Characterization and Homology Modeling of a Novel Water-Forming NADH Oxidase from *Streptococcus mutans* ATCC 25175. *Int. J. Biol. Macromol.* **2018**, *113*, 1073−1079.
(34) Sakamoto, M.; Uchimura, T.; Komagata, K. Comparison of H_2O-Forming NADH Oxidase from *Leuconostoc mesenteroides* subsp. *mesenteroides* NRIC 1541^T and H_2O_2-Forming NADH Oxidase from *Sporolactobacillus inulinus* NRIC 1133T. *J. Ferment. Bioeng.* **1996**, *82* (6), 531−537.
(35) Lountos, G. T.; Jiang, R.; Wellborn, W. B.; Thaler, T. L.; Bommarius, A. S.; Orville, A. M. The Crystal Structure of NAD(P)H Oxidase from *Lactobacillus sanfranciscensis*: Insights into the Conversion of O_2 into Two Water Molecules by the Flavoenzyme. *Biochemistry* **2006**, *45* (32), 9648−9659.
(36) Mallett, T. C.; Claiborne, A. Oxygen Reactivity of an NADH Oxidase C42S Mutant: Evidence for a C(4a)-Peroxyflavin Intermediate and a Rate-Limiting Conformational Change. *Biochemistry* **1998**, *37* (24), 8790−8802.
(37) Wu, R.; Zhu, Z. Self-Powered Enzymatic Electrosynthesis of L-3,4-Dihydroxyphenylalanine in a Hybrid Bioelectrochemical System. *ACS Sustainable Chem. Eng.* **2018**, *6* (10), 12593−12597.
(38) Sheldon, R. A.; Woodley, J. M. Role of Biocatalysis in Sustainable Chemistry. *Chem. Rev.* **2018**, *118* (2), 801−838.
(39) Danielsson, B.; Winqvist, F.; Malpote, J. Y.; Mosbach, K. Regeneration of NADH with Immobilized Systems of Alanine Dehydrogenase and Hydrogen Dehydrogenase. *Biotechnol. Lett.* **1982**, *4* (10), 673−678.
(40) Sheldon, R. A.; van Peltb, S. Enzyme Immobilisation in Biocatalysis: Why, What and How. *Chem. Soc. Rev.* **2013**, *42* (15), 6223−6235.
(41) Karyakin, A. A. Principles of Direct (Mediator Free) Bioelectrocatalysis. *Bioelectrochemistry* **2012**, *88*, 70−75.
(42) Ruff, A.; Conzuelo, F.; Schuhmann, W. Bioelectrocatalysis as the Basis for the Design of Enzyme-Based Biofuel Cells and Semi-Artificial Biophotoelectrodes. *Nat. Catal.* **2020**, *3* (3), 214−224.
(43) Chen, H.; Simoska, O.; Lim, K.; Grattieri, M.; Yuan, M.; Dong, F.; Lee, Y. S.; Beaver, K.; Weliwatte, S.; Gaffney, E. M.; Minteer, S. D. Fundamentals, Applications, and Future Directions of Bioelectrocatalysis. *Chem. Rev.* **2020**, *120* (23), 12903−12993.
(44) Chen, H.; Dong, F.; Minteer, S. D. The Progress and Outlook of Bioelectrocatalysis for the Production of Chemicals, Fuels and Materials. *Nat. Catal.* **2020**, *3* (3), 225−244.
(45) Atta, N. F.; Gawad, S. A. A.; El-Ads, E. H.; El-Gohary, A. R. M.; Galal, A. A New Strategy for NADH Sensing Using Ionic Liquid Crystals-Carbon Nanotubes/Nano-Magnetite Composite Platform. *Sens. Actuators, B* **2017**, *251*, 65−73.
(46) Moiroux, J.; Elving, P. J. Effects of Adsorption, Electrode Material, and Operational Variables on the Oxidation of Dihydronicotinamide Adenine Dinucleotide at Carbon Electrodes. *Sens. Actuators, B* **1978**, *50* (8), 1056−1062.
(47) Jaegfeldt, H. Adsorption and Electrochemical Oxidation Behaviour of NADH at a Clean Platinum Electrode. *J. Electroanal. Chem. Interfacial Electrochem.* **1980**, *110* (3), 295−302.
(48) Ali, I.; Omanovic, S. Kinetics of Electrochemical Reduction of NAD^+ on a Glassy Carbon Electrode. *Int. J. Electrochem. Sci.* **2013**, *8* (3), 4283−4304.
(49) Koochana, P. K.; Mohanty, A.; Subhadarshanee, B.; Satpati, S.; Naskar, R.; Dixitc, A.; Behera, R. K. Phenothiazines and Phenoxazines: As Electron Transfer Mediators for Ferritin Iron Release. *Dalton Trans.* **2019**, *48* (10), 3314−3326.
(50) Halder, S.; Mandal, S.; Kundu, A.; Mandal, B.; Adhikari, D. Super-Reducing Behavior of Benzo[B]Phenothiazine Anion under Visible-Light Photoredox Condition. *J. Am. Chem. Soc.* **2023**, *145* (41), 22403−22412.
(51) Lee, K. J.; Lodaya, K. M.; Gruninger, C. T.; Rountree, E. S.; Dempsey, J. L. Redox Mediators Accelerate Electrochemically-Driven Solubility Cycling of Molecular Transition Metal Complexes. *Chem. Sci.* **2020**, *11* (36), 9836−9851.
(52) Zhang, L.; Li, Y.; Li, D.-W.; Jing, C.; Chen, X.; Lv, M.; Huang, Q.; Long, Y.-T.; Willner, I. Single Gold Nanoparticles as Real-Time Optical Probes for the Detection of NADH-dependent Intracellular Metabolic Enzymatic Pathways. *Angew. Chem.* **2011**, *123* (30), 6921−6924.
(53) Sporty, J. L.; Kabir, M. M.; Turteltaub, K. W.; Ognibene, T.; Lin, S.-J.; Bench, G. Single Sample Extraction Protocol for the Quantification of NAD and NADH Redox States in Saccharomyces Cerevisiae. *J. Sep. Sci.* **2008**, *31* (18), 3202−3211.
(54) Ritov, V. B.; Menshikova, E. V.; Kelley, D. E. High-Performance Liquid Chromatography-Based Methods of Enzymatic Analysis: Electron Transport Chain Activity in Mitochondria from Human Skeletal Muscle. *Anal. Biochem.* **2004**, *333* (1), 27−38.
(55) Xie, W.; Xu, A.; Yeung, E. S. Determination of NAD^+ and NADH in a Single Cell under Hydrogen Peroxide Stress by Capillary Electrophoresis. *Anal. Chem.* **2009**, *81* (3), 1280−1284.
(56) Chen, J.; Wang, L.; Huang, Y.; Li, Z.; Zhang, H.; Ali, M. C.; Liu, J.; Chen, X.; Qiu, H. Fabrication of Nanoporous Graphene/Cuprous Oxide Nanocomposite and Its Application for Chemilumi-

https://doi.org/10.1021/jacsau.4c00528
JACS Au 2024, 4, 3581−3592

nescence Sensing of NADH in Human Serum and Cells. *Sens. Actuators, B* **2019**, *290*, 15−22.
(57) Hentall, P. L.; Flowers, N.; Bugg, T. D. Enhanced Acid Stability of a Reduced Nicotinamide Adenine Dinucleotide (NADH) Analogue. *Chem. Commun.* **2001**, *20*, 2098−2099.
(58) Fukazawa, K.; Ishihara, K. Enhanced Stability of NADH/Dehydrogenase Mixture System by Water-Soluble Phospholipid Polymers. *Biomater. Biomech. Bioeng.* **2016**, *3* (1), 37−46.
(59) Yamauti, J.-i.; Yoshimura, S.; Takagahara, I.; Fujii, K.; Tai, A.; Yamashita, J.; Horio, T. Isolation and Characterization of Two Potent Inhibitors of Various NADH Dehydrogenases Formed During Storage of NADH. *J. Biochem.* **1981**, *90* (4), 941−955.
(60) Vogt, S.; Schneider, M.; Schäfer-Eberwein, H.; Nöll, G. Determination of the pH Dependent Redox Potential of Glucose Oxidase by Spectroelectrochemistry. *Anal. Chem.* **2014**, *86* (15), 7530−7535.
(61) Batterjee, S. M.; Marzouk, M. I.; Aazab, M. E.; El-Hashash, M. A. The Electrochemistry of Some Ferrocene Derivatives: Redox Potential and Substituent Effects. *Appl. Organomet. Chem.* **2003**, *17* (5), 291−297.
(62) Ma, Y.; Jin, Z.; Peng, B.; Ding, J.; Wang, N.; Zhou, M. Investigation of Direct Electrooxidation Behavior of NADH at a Chemically Modified Glassy Carbon Electrode. *J. Electrochem. Soc.* **2015**, *162* (6), No. H317.
(63) Caserta, G.; Papini, C.; Adamska-Venkatesh, A.; Pecqueur, L.; Sommer, C.; Reijerse, E.; Lubitz, W.; Gauquelin, C.; Meynial-Salles, I.; Pramanik, D.; Artero, V.; Atta, M.; Del Barrio, M.; Faivre, B.; Fourmond, V.; Leger, C.; Fontecave, M. Engineering an [FeFe]-Hydrogenase: Do Accessory Clusters Influence O(2) Resistance and Catalytic Bias? *J. Am. Chem. Soc.* **2018**, *140* (16), 5516−5526.
(64) Fourmond, V.; Léger, C. Theoretical Understanding of the Penetration of O_2 in Enzymatic Redox Polymer Films: The Case of Unidirectional Catalysis and Irreversible Inactivation in a Film of Arbitrary Thickness. *ChemElectroChem* **2021**, *8* (13), 2607−2615.
(65) Yadav, S.; Haas, R.; Boydas, E. B.; Roemelt, M.; Happe, T.; Apfel, U. P.; Stripp, S. T. Oxygen Sensitivity of [FeFe]-Hydrogenase: A Comparative Study of Active Site Mimics inside Vs. Outside the Enzyme. *Phys. Chem. Chem. Phys.* **2024**, *26* (28), 19105−19116.
(66) Fasano, A.; Fourmond, V.; Leger, C. Outer-Sphere Effects on the O(2) Sensitivity, Catalytic Bias and Catalytic Reversibility of Hydrogenases. *Chem. Sci.* **2024**, *15* (15), 5418−5433.
(67) del Barrio, M.; Guendon, C.; Kpebe, A.; Baffert, C.; Fourmond, V.; Brugna, M.; Léger, C. Valine-to-Cysteine Mutation Further Increases the Oxygen Tolerance of *Escherichia coli* NiFe Hydrogenase HYD-1. *ACS Catal.* **2019**, *9* (5), 4084−4088.
(68) Fasano, A.; Guendon, C.; Jacq-Bailly, A.; Kpebe, A.; Wozniak, J.; Baffert, C.; Barrio, M. D.; Fourmond, V.; Brugna, M.; Leger, C. A Chimeric NiFe Hydrogenase Heterodimer to Assess the Role of the Electron Transfer Chain in Tuning the Enzyme's Catalytic Bias and Oxygen Tolerance. *J. Am. Chem. Soc.* **2023**, *145* (36), 20021−20030.
(69) Kubas, A.; Orain, C.; De Sancho, D.; Saujet, L.; Sensi, M.; Gauquelin, C.; Meynial-Salles, I.; Soucaille, P.; Bottin, H.; Baffert, C.; Fourmond, V.; Best, R. B.; Blumberger, J.; Leger, C. Mechanism of O(2) Diffusion and Reduction in Fefe Hydrogenases. *Nat. Chem.* **2017**, *9* (1), 88−95.
(70) Orain, C.; Saujet, L.; Gauquelin, C.; Soucaille, P.; Meynial-Salles, I.; Baffert, C.; Fourmond, V.; Bottin, H.; Leger, C. Electrochemical Measurements of the Kinetics of Inhibition of Two FeFe Hydrogenases by O_2 Demonstrate That the Reaction Is Partly Reversible. *J. Am. Chem. Soc.* **2015**, *137* (39), 12580−12587.
(71) Winkler, M.; Duan, J.; Rutz, A.; Felbek, C.; Scholtysek, L.; Lampret, O.; Jaenecke, J.; Apfel, U. P.; Gilardi, G.; Valetti, F.; Fourmond, V.; Hofmann, E.; Leger, C.; Happe, T. A Safety Cap Protects Hydrogenase from Oxygen Attack. *Nat. Commun.* **2021**, *12* (1), No. 756.
(72) Goldet, S. T. S. G.; Sanganas, C. B. O.; Vincent, K. A.; Haumann, M.; Happe, F. A. A. T.; et al. How Oxygen Attacks [FeFe] Hydrogenases from Photosynthetic Organisms. *Proc. Natl. Acad. Sci. U.S.A.* **2009**, *106* (41), 17331−17336.
(73) Zheng, Y.-C.; Xu, J.-H.; Wang, H.; Lin, G.-Q.; Hong, R.; Yu, H.-L. Hydroxynitrile Lyase Isozymes from Prunus Communis: Identification, Characterization and Synthetic Applications. *Adv. Synth. Catal.* **2017**, *359* (7), 1185−1193.
(74) Lazanas, A. C.; Prodromidis, M. I. Electrochemical Impedance Spectroscopy-a Tutorial. *ACS Meas. Sci. Au* **2023**, *3* (3), 162−193.

https://doi.org/10.1021/jacsau.4c00528
JACS Au 2024, 4, 3581−3592